

Ordering Surfaces on the Nanoscale: Implications for Protein Adsorption

Andrew Hung,[‡] Steve Mwenifumbo,[‡] Morgan Mager,[‡] Jeffrey J. Kuna,[§] Francesco Stellacci,[§] Irene Yarovsky,^{*,‡} and Molly M. Stevens^{*,‡}

[‡]Department of Materials, Department of Bioengineering, and Institute for Biomedical Engineering, Imperial College London, London, U.K., SW7 2AZ

[‡]Health Innovations Research Institute, School of Applied Sciences, RMIT University, GPO Box 2476 V, Melbourne, Victoria, Australia, 3001

[§]Department of Materials Science and Engineering, Massachusetts Institute of Technology, Cambridge, Massachusetts 02139, United States

 Supporting Information

ABSTRACT: Monolayer-protected metal nanoparticles (MPMNs) are a newly discovered class of nanoparticles with an ordered, striped domain structure that can be readily manipulated by altering the ratio of the hydrophobic to hydrophilic ligands. This property makes them uniquely suited to systematic studies of the role of nanostructuring on biomolecule adsorption, a phenomenon of paramount importance in biomaterials design. In this work, we examine the interaction of the simple, globular protein cytochrome C (Cyt C) with MPMN surfaces using experimental protein assays and computational molecular dynamics simulations. Experimental assays revealed that adsorption of Cyt C generally increased with increasing surface polar ligand content, indicative of the dominance of hydrophilic interactions in Cyt C-MPMN binding. Protein–surface adsorption enthalpies calculated from computational simulations employing rigid-backbone coarse-grained Cyt C and MPMN models indicate a monotonic increase in adsorption enthalpy with respect to MPMN surface polarity. These results are in qualitative agreement with experimental results and suggest that Cyt C does not undergo significant structural disruption upon adsorption to MPMN surfaces. Coarse-grained and atomistic simulations furthermore elucidated the important role of lysine in facilitating Cyt C adsorption to MPMN surfaces. The amphipathic character of the lysine side chain enables it to form close contacts with both polar and nonpolar surface ligands simultaneously, rendering it especially important for interactions with surfaces composed of adjacent nanoscale chemical domains. The importance of these structural characteristics of lysine suggests that proteins may be engineered to specifically interact with nanomaterials by targeted incorporation of unnatural amino acids possessing dual affinity to differing chemical motifs.



Monolayer-protected metal nanoparticles (MPMNs) are a newly discovered class of nanoparticles with an ordered, striped domain structure that can be readily manipulated by altering the ratio of the hydrophobic to hydrophilic ligands. This property makes them uniquely suited to systematic studies of the role of nanostructuring on biomolecule adsorption, a phenomenon of paramount importance in biomaterials design. In this work, we examine the interaction of the simple, globular protein cytochrome C (Cyt C) with MPMN surfaces using experimental protein assays and computational molecular dynamics simulations. Experimental assays revealed that adsorption of Cyt C generally increased with increasing surface polar ligand content, indicative of the dominance of hydrophilic interactions in Cyt C-MPMN binding. Protein–surface adsorption enthalpies calculated from computational simulations employing rigid-backbone coarse-grained Cyt C and MPMN models indicate a monotonic increase in adsorption enthalpy with respect to MPMN surface polarity. These results are in qualitative agreement with experimental results and suggest that Cyt C does not undergo significant structural disruption upon adsorption to MPMN surfaces. Coarse-grained and atomistic simulations furthermore elucidated the important role of lysine in facilitating Cyt C adsorption to MPMN surfaces. The amphipathic character of the lysine side chain enables it to form close contacts with both polar and nonpolar surface ligands simultaneously, rendering it especially important for interactions with surfaces composed of adjacent nanoscale chemical domains. The importance of these structural characteristics of lysine suggests that proteins may be engineered to specifically interact with nanomaterials by targeted incorporation of unnatural amino acids possessing dual affinity to differing chemical motifs.

INTRODUCTION

Interfacial energy plays a fundamental role in biological processes at solid–liquid interfaces,^{1–3} and consequently, much research has been devoted to understanding its influence on processes such as protein adsorption.⁴ Unfortunately, an accepted framework providing a global and quantitative understanding of nanoscale structure–property relationships connecting interfacial energy to the degree/specificity of protein adsorption is still lacking. This important and unresolved issue is of practical significance, since protein adsorption is one of the first biological responses to a surface (after water–surface interactions). As such, this process dictates biospecificity and, therefore, utility in a wide range of applications (e.g., bioassays, biosensors, drug delivery, and medical devices).

Nanoparticles (NPs) offer the potential to elucidate fundamental properties of biological interactions at the nano- and molecular-scale, particularly when protected with self-assembled monolayers (SAMs). Monolayer-protected metal nanoparticles (MPMNs) are supramolecular assemblies comprising a SAM organized around

a nanosized metallic core, typically thiolated molecules assembled on a gold core.⁵ Recent studies^{6–11} investigating MPMNs composed of binary mixtures of hydrophobic and hydrophilic ligands observed striped ligand shells structured with alternating 0.5–2 nm thick hydrophobic and hydrophilic domains. Subsequent investigation has indicated that the formation of these domains is due to unique entropic and enthalpic effects of packing a 2D crystal structure onto a highly curved surface.^{12,13}

These striped domains are so thin (commensurate with the size of solvent molecules) that the structure or ‘order’ leads to unanticipated surface properties that cannot be explained by bulk composition alone. For example, in a study by Centrone et al.,⁷ the ligand shell morphology of mixed SAMs on NPs was observed to affect the NP solubility almost as much as molecular composition. More recently it was shown that MPMN films exhibited a non-monotonic dependence of wettability on composition. Simulation

Received: September 14, 2010

Published: January 5, 2011

results of that system indicate that the surface free energy could vary significantly as a function of ordering even at a fixed composition. These findings represent a deviation from conventional continuum thermodynamic predictions that generally treat multicomponent surfaces as a function of average surface composition.¹⁴ Results from these wettability experiments on local surface organization of nano-scale structures have contributed to ongoing experimental and computational studies into interfacial energy.¹⁵ Given that proteins and other biological structures exhibit nano-scale patterning of hydrophobic/hydrophilic species, these findings should have significant implications for the study of biological processes such as protein adsorption.

With this possible relationship in mind, we have extended our computational and experimental studies to examine the role of nano-scale domains on protein adsorption. To gain insight into these interactions, we studied the adsorption of cytochrome C (Cyt C) onto mixed MPMNs with striped hydrophilic/hydrophobic domains less than 2 nm in width. We experimentally determined the extent of adsorption of Cyt C onto MPMNs with varying surface ligand composition by microBCA assays. We subsequently applied molecular dynamics (MD) simulations to study Cyt C adsorption onto the surfaces of MPMNs, employing coarse-grained (CG) representations of the protein and nanoparticle models. Our simulations offer further insights into the molecular mechanisms of protein–MPMN binding, enabling an identification of the principal binding orientations of the protein, which was found to be strongly dependent on surface composition. Cyt C was selected for this study due to its relatively small size and known structural stability upon surface adsorption.^{16,17} It therefore serves as an ideal protein for this prototype study, as its MPMN adsorption behavior is dominated by interactions with surface-exposed residues of the protein in its native folding state, the structure of which is well-characterized. Furthermore, the stability of Cyt C means that a semirigid body approach (distance-restrained backbone beads, described below, Molecular Dynamics Simulations) is a valid representation of the protein, a necessity for our implementation of the CG model, which enables the rapid dynamical exploration of translation/rotational motion of the protein with respect to surfaces. We also employ an all-atom forcefield approach to examine the adsorption of Cyt C on model MPMN surfaces, with initial protein orientations based on those obtained from the CG simulations. Use of a combined, multiscale approach, allows the exploitation of the individual advantages conferred by both types of models. The CG simulations enabled an unbiased determination of favorable binding orientations on the MPMN surfaces, while atomistic models of the protein–surface systems enabled elucidation of specific residue–ligand interactions at the atomic level.

MATERIALS AND METHODS

NP Synthesis and Characterization. All the precursors and solvents were used as received without any further purification. Chloro-(triphenylphosphine) gold(I), 6-mercapto-1-hexanol (MH), 1-octanethiol (OT), borane *tert*-butylamine complex, 3-mercaptopropyl trimethoxysilane (MPTMS), sulphuric acid, Tween 20, cytochrome c (Cyt C), and phosphate buffered saline (PBS; 137 mM NaCl, 2.7 mM KCl, pH 7.4) were purchased from Sigma-Aldrich, U.K. Hydrogen peroxide, and 1,9-nonanedithiol were purchased from Alfa, U.K. The remaining solvents, including ethanol (EtOH), acetone, isopropyl alcohol, diethyl ether (Et₂O), dichloromethane (DCM), toluene, and benzene were purchased from VWR, U.K. Carbon coated Cu TEM grids (300 mesh) were purchased from Agar Scientific, U.K.

Five different types of monolayer-protected gold NPs (coated with varying stoichiometric ratios of MH and OT ligands) were synthesized: 100% OT, 2:1 MH:OT, 1:1 MH:OT, 1:2 MH:OT, and 100% MH.⁹ The MH and OT coated gold NPs were synthesized using a slightly modified one-phase method.¹⁸ See Supporting Information for further NP synthesis and characterization details.

Substrate Modification and MPMN Film Assembly. Borosilicate glass substrates (VWR, 75 × 25 × 1 mm slides and 13 mm diameter coverslips) were rinsed with EtOH then immersed in piranha (4:1 H₂SO₄/35% H₂O₂) for 45 min. The substrates were then rinsed with deionized H₂O, followed by isopropyl alcohol, and dried in a stream of N₂.

One set of substrates was prepared for use as 2D flat SAM control surfaces. Electron beam vapor deposition (EBVD) was used to deposit first a 5 nm thick Cr layer and then a 25 nm thick gold layer using a Denton DV-502A electron beam evaporator (Denton Vacuum). The EBVD gold-coated substrates were rinsed with H₂O and EtOH, and dried with N₂. SAMs were then prepared on these surfaces using established methods.²⁶ Briefly, the substrates were placed in ethanolic solutions (total thiol concentrations of 10 mM) for 7 days, at which point they were rinsed with EtOH and dried with N₂.

A second set of substrates was functionalized in an evacuated desiccator with an open vial of MPTMS for 90 min¹⁹ and subsequently used to fabricate the MPMN films using established layer-by-layer assembly techniques.^{20–22} The MPTMS-functionalized substrates were rinsed with copious amounts of EtOH then placed in NP solutions (0.375 mg/mL) for 48 h. Substrates were then removed, rinsed profusely with EtOH, transferred to 5 mM ethanolic solutions of 1,9-nonanedithiol for 2 h, rinsed with EtOH, and placed back into the NP solutions. Subsequent layers were produced via the same procedure but with a 24 rather than 48 h incubation with NPs. The pure OT NP coated slides were rinsed with the solvent of the previous solution followed by rinsing with the solvent used in the upcoming solution. This procedure was repeated five times on each sample. Film growth was monitored using UV–vis spectroscopy.

Substrate Characterization. After synthesis, these surfaces were characterized by AFM and contact angle measurements to determine roughness and surface energy, respectively. AFM imaging was performed using a Digital Instruments Nanoscope IIIa AFM (Veeco Instruments) operated in the tapping mode. The AFM images of square 5 μm scans were acquired with a scan rate of 1 Hz and a sampling rate of 512 lines under ambient conditions and are presented in Supporting Information, Figure S2. The wettability of the specimens was determined using sessile drop techniques. A drop shape analysis system (EasyDrop DSA20E, Kruss, Germany) with analysis software (DSA1 version 1.80, Kruss, Germany) was used to measure contact angles, θ_{CA} , for the various specimens. At least 12 measurements (5 μL H₂O drops at a rate of 6 μL/min) were made on each of the prepared surfaces. All experiments were performed under ambient conditions. Final θ_{CA} for wettability comparisons are reported as averages ± standard deviation. From the contact angle measurements, the work of adhesion (W_{SL}) was calculated using the Young–Dupré equation.²³

Protein Adsorption. We have studied the adsorption of Cyt C onto the MPMNs. Single protein solutions of Cyt C were prepared by dilution in PBS at a concentration of ~20 μg/mL. The total protein adsorption was assessed using a commercially available microBCA assay (Pierce Biotechnology).²⁴ A modified version of the standard microBCA assay protocol²⁴ was used on the rectangular specimens fitted with silicone flexiPERM Micro12 gaskets (Sigma, U.K.). Briefly, the specimens were incubated with the prepared single protein solutions at 37 °C for 2 h. Following the incubation period, the supernatant was removed and the specimens were rinsed three times with a 0.05% (v/v) Tween 20 in PBS solution. Next, the microBCA assay working reagent was added to each of the wells and incubated for another 2 h at 37 °C. The specimens were then

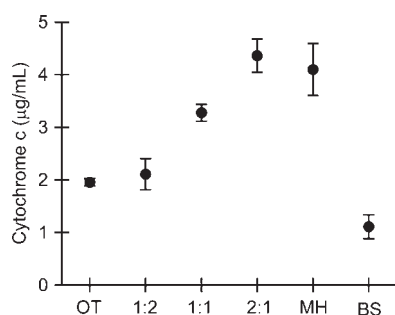


Figure 1. MicroBCA measures of Cyt C adsorption on MPMN with respect to ligand composition. Ligand composition was varied from pure octanethiol (OT) to pure mercaptohexanol (MH). For comparison, the adsorption on borosilicate glass controls (BS) is also shown. Values shown are average \pm standard deviation.

removed from the incubator and the contents of the wells were transferred to 96 well plates. Adsorption was measured at a wavelength of 570 nm using an Anthos 2020 microplate reader (Biochrom Limited, U.K.). Total protein content was then determined by comparing the optical density of the specimens with known standard concentrations of the protein. Calibration measurements were also attempted using X-ray photoelectron spectroscopy (XPS), but the results were found to be more variable and less reliable than those obtained from the microBCA assay. This finding is consistent with previous studies that have shown that XPS is more appropriate for qualitative (rather than quantitative) surface characterization in protein adsorption studies.²⁵

Molecular Dynamics Simulations. Coarse-Grained Simulations. CG MD simulations were performed on Cyt C-nanoparticle systems using GROMACS version 3.3^{26,27} using the coarse-grained (CG) MARTINI force field developed by Marrink et al.^{28,29} Simulation time steps of 10 fs were applied to integrate the equations of motion. Forcefield parameters for the MPMNs models with different ligand compositions and nanostructures were derived from existing parameters for modeling lipids.^{29,30} Monolayer ligands are modeled with 3 beads connected consecutively with harmonic potentials. For the CG OT model, four (atomistic) methylene units are combined into each of 2 tail beads, and the headgroup (the group attached directly to the NP surface) is represented by a single polar (P1) bead (Supporting Information, Figure S4). Each of the two harmonic bonds has an equilibrium length of 0.47 nm. A similar model is adopted for the CG MH, except the group at the end of the tail is represented by a single P1 bead. The equilibrium bond connecting the chain beads was set at 0.37 nm to reflect the shorter chain length of (atomistic) MH compared to OT. Gold NP atoms were modeled as strongly hydrophobic (C1) beads. Each CG water bead represents four molecules. Ions are modeled using reduced charges of ± 0.7 to mimic the implicit electrostatic screening by the first hydration shell, as described in Monticelli et al.²⁹

To investigate the effects of domain size and local hydrophilic/hydrophobic ordering on protein adsorption dynamics, we carried out simulations of Cyt C MH:OT striped MPMNs of different compositions: OT Homo (0% MH); 1:2 MH:OT (33% MH); 1:1 MH:OT (50% MH) 'thin' (1 ligand wide); 1:1 MH:OT (50% MH) 'thick' (2 ligands wide); 2:1 MH:OT (67% MH); and 100% MH, with MH stripe widths of 0.6, 0.6, 1.0, 1.4 nm, respectively, for the mixed MPMN. The surface ligand nanostructures are qualitatively based on previous theoretical and experimental studies¹⁵ which indicate the formation of ordered ripples. The MPMNs modeled are outlined and illustrated in Figure 1. We have explored two structural possibilities for the 1:1 MH:OT MPMN: (1) single-molecule ('thin') and (2) two-molecule wide ('thick') stripes. We note that the 'thick' 1:1 MPMN model is more consistent with the mean STM-obtained value of ~ 8 Å (suggestive of a stripe width of more than 1 ligand), and this is reflected in the better agreement of our simulations with current experimental data for this particular MPMN

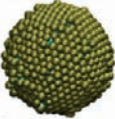
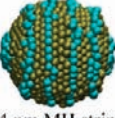
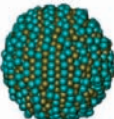
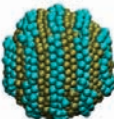
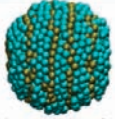

(see Results and Discussion below). Furthermore, we have calculated the surface ligand–ligand interaction energies (i.e., between OT–OT, OT–MH and MH–MH ligands) of both "thick" and "thin" striped 1:1 MH:OT surfaces. We find that the "thick" surface has $\sim 10\%$ lower enthalpy than the "thin," suggesting that both forms are likely to co-exist although the "thick" isoform may be marginally more stable. Consideration of both isoforms is particularly useful since it allows comparison of two surfaces with the same ligand composition but different stripe widths, enabling us to determine the influence of nanostructure on protein adsorption, free from possible confounding effects due to variations in total surface hydrophobicity.

The CG model of Cyt C was derived from the protein coordinates from PDB ID 2I89, 1hrc³¹ obtained from the RCSB (www.rcsb.org).³² MD simulations were performed using parameters derived from the MARTINI amino acids forcefield v2.1.²⁹ Distance restraints were placed between the backbone beads of the protein in order to maintain its native fold. This model allows us to study the *initial* binding of proteins to surfaces prior to significant conformational changes (possibly) induced by interactions with the surfaces. This approximation is likely to be reasonable for Cyt C, which is known to largely preserve its native fold after adsorption onto a number of different surfaces.^{16,17} Further details of the MPMNs, CG protein models, and simulation parameters are provided in Supporting Information.

We have simulated the binding of Cyt C to each of the 6 MPMN particles by placement of the protein with different initial orientations within proximity of the NP surface, followed by solvation of the simulation cell with CG water particles (P1 beads), and addition of cations and anions to ensure charge neutrality and maintain ~ 110 mM ionic concentration to mimic experimental conditions. Initial cell dimensions were $16 \times 16 \times 16$ nm³, with fluctuations of ~ 0.5 nm during the course of the trajectories. After system construction, we performed energy minimization using the steepest-descent algorithm with step-sizes of 0.01 nm to remove close atomic contacts. This was followed by simulation of 800 ns in effective time; see Marrink et al. for a discussion of CG time scales.³⁰ For each protein–MPMN pair, we performed simulations with four different initial protein orientations (illustrated in Figure S4, Supporting Information) with respect to the surface in order to enhance conformational sampling. The initial orientation is identical for each MPMN system with the same number label. In total, we performed 24 CG simulations.

Atomistic Simulations. Atomistic simulations were performed on Cyt C-model MPMN surface systems using the atomistic GROMOS96 forcefield with the 53A6 parameter set^{33,34} (further simulation parameters are given in Supporting Information). The protein model was based on horse heart Cyt C (2I89, 1hrc³¹). We have simulated the adsorption of Cyt C on four (4) model MPMN surfaces: (1) homogeneous OT; (2) 1:1 MH:OT 'thin'; (3) 1:1 MH:OT 'thick'; and (4) homogeneous MH. The MPMNs were modeled as planar surfaces, with alternating linear stripes of OT and MH for the 1:1 mixed-composition surfaces. Planar interfaces are expected to provide reasonable approximations to the (curved) MPMN surfaces, owing to the relatively low curvature of the MPMN (~ 3.2 nm radius) compared to that of Cyt C (~ 1.2 nm radius of gyration). The true extent to which flat surfaces are accurate representations of MPMNs is explored further in Results and Discussion, Atomistic Simulations of Cyt C Adsorption. The stripe widths correspond approximately to those used in the CG simulations, being 0.6 and 0.92 nm wide for the 'thin' and 'thick' MPMNs, respectively. The OT ligands are modeled as octane, while MH ligands are modeled as hexanol. The ligands are oriented such that the C1 united atoms (corresponding to the first CH₃ group in both ligands) are exactly aligned along the XY plane, with the long axes of the ligands oriented parallel to the z-axis (surface normal) and the terminal CH₃ of OT and terminal OH group of MH placed in the "positive" z-direction (above the C1). Throughout the simulations, the C1 atoms were positionally

Table 1. Physicochemical and Morphological Properties of MPMN Surfaces

Surface Type	MPMNs		Surface Properties	
	Ligand Shell Morphology ^a	Core Size ^b (nm)	Contact Angle θ_{CA} ($^{\circ}$) ^c	Work of Adhesion W_{SL} (mN/m)
MH Homo (100% MH)	 homogeneous	5.1 ± 1.1	45.7 ± 10.4	122.8 ± 9.3
2:1 MH:OT (67% MH)	 1.4 nm MH stripes	4.6 ± 1.2	41.3 ± 2.5	126.6 ± 2.1
1:1 MH:OT (50% MH)	 'Thin' 0.6 nm MH stripes	4.5 ± 0.9	67.2 ± 6.6	100.3 ± 7.7
	 'Thick' 1.0 nm MH stripes			
1:2 MH:OT (33% MH)	 0.6 nm MH stripes	4.5 ± 0.8	51.2 ± 2.5	117.6 ± 2.5
OT Homo (0% MH)	 homogeneous	4.9 ± 0.9	84.9 ± 5.2	78.7 ± 6.5

^a Schematic drawings of NPs in which the cyan beads represent OT molecules and bronze beads represent MH molecules. MH stripe width was estimated from STM studies. ^b Determined from TEM images and expressed as average diameter ± standard deviation. ^c Data were originally published by Kuna et al.¹⁵ and are reproduced here for comparison purposes.

constrained in order to model ligand immobilization on MPMN surfaces. For each simulation, Cyt C was initially placed in close proximity to the model MPMN surfaces, with the closest contact atom of the protein within 5 Å of the C8 and OH groups of OT and MH. The initial orientation for each system was selected based on the lowest (most negative) binding enthalpy orientation identified from CG simulations (see Results and Discussion). The simulation box sizes for the systems are: (1) OT, 6.0 × 6.3 × 7.4 nm; (2) 1:1 'thin', 6.0 × 6.0 × 7.4 nm; (3) 1:1 'thick', 6.0 × 5.4 × 7.4 nm; and (4) MH, 6.0 × 6.3 × 7.4 nm. The Cyt C-surface systems thereby constructed were subsequently solvated using SPC water³⁵ and charge-neutralizing Na⁺. The solvated systems were energy-minimized using the steepest descent algorithm implemented in GROMACS, followed by 100 ps of solvent-equilibration simulation in which the non-H atoms of Cyt C were positionally restrained. Subsequently, 50 ns of unrestrained simulation trajectories were collected for each of the four systems. The final frames from the simulations are illustrated in Figure 7A-D.

Statistical Analysis. The statistical analysis was performed using SYSTAT (Systat Software) and SPSS software packages (SPSS, Inc.). Unless otherwise stated, data are presented as mean ± standard deviation. A nonparametric Mann–Whitney U test was used to statistically assess differences in protein adsorption and interaction enthalpies between the different MPMN and control surfaces. These differences were regarded as significant if $P < 0.05$. Linear regression analysis was applied to compare differences between experimental and simulated data.

RESULTS AND DISCUSSION

MPMN Film Protein Adsorption. We have performed protein adsorption measurements on films comprising the five MPMN compositions described in Materials and Methods above. Total protein content was investigated using microBCA, a method that has been shown to reliably quantify protein adsorption on surfaces,^{36,37} in particular on nanomaterial interfaces.³⁸ It is important to note that part of the adsorbed protein layer may have been removed due to the rinse and measure methods used to quantify protein adsorption in this work. We therefore make the underlying assumption that the protein adsorption values represent the irreversibly bound fraction of proteins that have not rinsed off. Figure 1 details the amount of Cyt C adsorbed onto the MPMN surfaces, with the control value of adsorption on to borosilicate glass given for comparison. In general, Cyt C exhibited increased protein adsorption with increasing mole fraction of MH (hydrophilic). On all the MPMN surfaces, Cyt C showed enhanced binding compared to the borosilicate controls, monotonically increasing with MH mole fraction/domain width (Figure 1).

Molecular Dynamics Simulations. We have investigated a series of MPMNs varying from purely hydrophilic to purely hydrophobic ligands, with surface compositions corresponding to those described above, shown in Table 1. Previous molecular simulations have examined the interactions between MPMN surfaces and water. Kuna et al.¹⁵ elucidated the molecular basis of

the nonmonotonic behavior of surface energy with respect to ligand composition on nanostructured MPMN surfaces. The interfacial solvent structure and energy were found to be strongly influenced by the formation of water clathrate structures in the vicinity of hydrophobic domains and the confinement of solvent molecules over hydrophilic domains. In the present work, we extend simulation studies to the interactions between MPMN surfaces and a protein, using a semirigid CG model of Cyt C and the nanoparticles, in order to further elucidate the influence of domain spacing effects on protein adsorption energies and orientation.

Cyt C–MPMN Binding Enthalpies. We carried out MD simulations to examine the interaction of a single Cyt C molecule with each of the six different nanostructured single MPMNs described in Table 1. In particular, we sought to identify the most favorable orientation on each MPMN type, residue-specific surface interactions, and protein–NP binding enthalpies. We define binding enthalpies as the sum of (nonbonded) interactions between the protein and NP CG beads. In the course of the simulations, the protein undergoes reorientation and translation along the NP surface, resulting in final (at 800 ns), surface-adsorbed orientations which differ from (but depend on) the initial prespecified positions. For most simulations, rotational/translational motions of the proteins are manifested in commensurate downward drifts in the protein–NP interaction enthalpies with respect to simulation time (data not shown), except for those that desorb. However, all simulations exhibit stabilized interaction enthalpies in the final 200 ns of their trajectories, fluctuating around an average value. The plateau-like behavior of the binding enthalpy time series within the considered time frame is also indicated by the similarities in standard deviations for the simulations. The observed structural/energetic drifts and subsequent plateau suggest that the CG model employed enables proteins to undergo sufficient diffusion to reach *local* energy minima. Multiple simulations increased the likelihood of identifying the low energy binding conformations representative of those found in the real systems. Table 2 shows the interaction enthalpies \pm standard deviation averaged over the final 200 ns of the trajectories.

Inspection of Table 2 reveals that the *lowest* binding enthalpy for each protein–NP system increases with respect to MH mole fraction from 0 to 100%MH if we assume a ‘thick-striped’ nanostructure for the 1:1 MH:OT surface. In particular, the Cyt C simulations exhibit linear, monotonic increases with respect to %MH, with increments of ~ 60 – 70 kJ/mol per 17% MH. Assuming that the real 1:1 MH:OT MPMN comprises ‘thick’ stripes, qualitative agreement is obtained with the experimentally acquired microBCA data, which generally exhibit increased % protein adsorption with increasing MH mole fraction. A notable exception is the homoligand MH MPMN, which exhibits a slightly lower average Cyt C adsorption compared to that of the 66%MH MPMN. However, an accurate determination of the order of the binding affinities of Cyt C on the 66% and 100% MH surfaces is difficult to ascertain from the present experimental data, due to the fact that the experimental error is comparable to the absolute difference in the average Cyt C adsorption values between the two surfaces. We also note that there are likely to be differences between the simulated and experimental systems which may result in quantitative discrepancies between simulated and measured binding affinities. For example, in the experimental systems, oligomer formation/

Table 2. Binding Enthalpies of Simulated Protein–NP Systems^a

system		Cyt C–NP binding enthalpy (kJ/mol) ^b
OT Homo	Orientation 1	-120 ± 17
	2	-94 ± 20
	3	-65 ± 18
	4	<u>-166 ± 19</u>
1:2 MH:OT	1	<u>-232 ± 16</u>
	2	-162 ± 16
	3	<u>-223 ± 13</u>
	4	-201 ± 14
1:1 MH:OT ‘thin’ stripes	1	<u>-179 ± 19</u>
	2	<u>-185 ± 14</u>
	3	-109 ± 17
	4	-164 ± 14
1:1 MH:OT ‘thick’ stripes	1	^c
	2	-192 ± 17
	3	-212 ± 11
	4	<u>-312 ± 19</u>
2:1 MH:OT	1	-245 ± 16
	2	<u>-369 ± 17</u>
	3	-284 ± 15
	4	-284 ± 20
MH Homo	1	-271 ± 20
	2	-314 ± 30
	3	-407 ± 20
	4	<u>-485 ± 28</u>

^a Lowest binding enthalpy values are highlighted in boldface and underlined. Values for next-lowest binding enthalpies are also highlighted if their values are within ~ 20 kJ/mol of the lowest binding enthalpy. ^b Average \pm standard deviation calculated over the final 200 ns of trajectory. ^c Protein desorbed from the NP surface in the course of the simulation.

adsorption on the surfaces may be present but is beyond the scope of our present computational models.

The correlation between experimental adsorption data and calculated binding enthalpies is demonstrated in Figure 2. Although binding enthalpies do not completely determine adsorption capacity, both the experimental assays and computational binding enthalpies indicate that the degree of protein attraction to the NP surface is proportional to hydrophilic ligand content, and therefore suggests that Cyt C–MPMN binding is dominated by hydrophilic interactions, in part due to the abundance of hydrophilic residues on the Cyt C surface (in the CG model employed, all such interactions are treated as attractive Lennard–Jones interactions with the degree of attraction determined by the LJ parameters). Of especial interest is the significant contribution of Lys to Cyt C–MPMN interactions, discussed in detail below (Binding Residues and the Role of Lysine).

Within two of the Cyt C–MPMN systems (i.e., 1:2 MH:OT and thin striped 1:1 MH:OT MPMN systems, see Table 2), the second-lowest binding enthalpies exhibit values which are within ~ 20 kJ/mol of the lowest binding enthalpy, indicating the existence of multiple, energetically favorable and (taking into account fluctuations at 300K) nearly energetically equivalent binding orientations. Given that protein function/bioactivity is

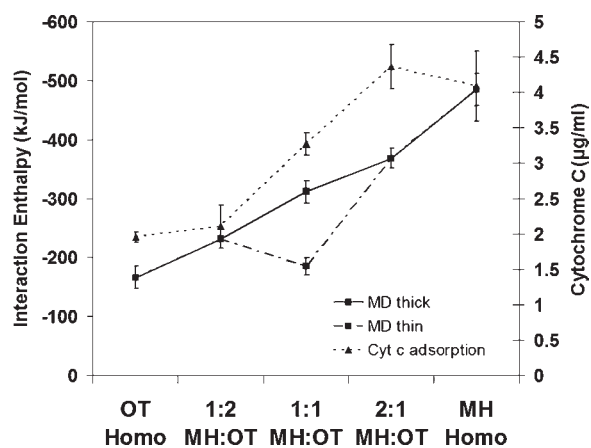


Figure 2. Comparison of lowest binding Cyt C–NP interaction enthalpies with experimental microBCA protein adsorption experiments (initial Cyt C concentration of $\sim 20 \mu\text{g}/\text{mL}$ with an incubation time 2 h at 37°C). Both the experimental and theoretical investigations show a monotonically increasing trend toward stronger adsorption at higher mole fractions of MH.

governed by specific motifs within its structure, different adsorbed conformations will therefore present different functional sites. Surfaces which promote multiple energetically favorable protein binding orientations may produce behaviors and properties which are consistent with a combination of the major orientations. For Cyt C, orientation of heme with respect to the surface template will determine its electron transfer pathway, and thus possibly influence its capability for conduction upon surface adsorption. Except for 1:2 MH:OT and MH homo systems, our simulations suggest that Cyt C binds to MPMN surfaces via the heme crevice with heme lying perpendicular to the surface plane. Thus, upon interaction with a solution of Cyt C, we might expect differences in protein-mediated surface electron conduction properties for the 1:2 and MH homo MPMNs compared to others studied in the present work.

The qualitative agreement between experiments and simulations also suggests that Cyt C does not deform significantly after adsorption to the MPMNs. This is supported by a number of studies of Cyt C on different types of surfaces. For example, Castellini et al.¹⁷ found that Cyt C adsorbed on kaolinite retains its catalytic activity, while Eggleston et al.¹⁶ reported that while Cyt C strongly adsorbs onto hematite surfaces, cyclic voltammetry measurements indicate redox potentials characteristic of the protein in a native conformational state. Studies of Cyt C adsorption on membrane bilayers showed shallow penetration, also with no evidence of significant misfolding.^{39–41}

Cyt C Binding Orientations. Figure 3 presents molecular graphics depicting the lowest-energy binding conformations for Cyt C on the different MPMNs, while Figure 3 and Table 3 summarize the atomic contact data associated with the various Cyt C residues and MPMN surface ligands. The hydrophobic OT homoligand surface (Figure 3A) finds Cyt C adsorbed via a region near the ‘heme crevice’, a partially open region which exposes one edge of the internal heme group, in agreement with the modeling work performed by Trzaskowski et al.⁴² who also predicted contact between isoleucine-81 and the surface for Cyt C adsorption on methyl-terminated SAMs. For the hydrophilic MH homoligand surface (Figure 3F), our simulations indicate that Cyt C adsorbs most favorably with horizontal orientation of the heme group and a cluster of Lys side chains in contact with

the surface, in good agreement with the model of Talasz et al.,⁴³ who determined favorable adsorption geometries on a model membrane surface (i.e., a surface which also presents hydrophilic groups to the adsorbed protein). Interestingly, our computational results also find agreement with previous experimental studies of Cyt C adsorption on homoligand MPMNs by Bayraktar et al.⁴⁴ In that study, NMR investigation revealed that Cyt C binds via its ‘front face’ on hydrophobic nanoparticle surfaces, a region on the protein in the vicinity of the heme crevice, which includes Phe82. This result is qualitatively consistent with our predicted binding orientation for Cyt C on the OT homoligand and 2:1 MH:OT MPMN surfaces (Figure 3A,C). Furthermore, their work also revealed that a much larger proportion of the surface around the heme crevice is solvent protected upon adsorption onto hydrophilic MPMNs as compared to hydrophobic MPMNs. This is qualitatively consistent with our results in two respects. First, our simulations show that a greater number of residues are in direct contact with the homoligand MH surface (Figure S5) compared to the other surfaces. Second, our simulations also predict multiple binding orientations that have similar interaction enthalpies, suggestive of the possibility that Cyt C can adopt multiple, equally favorable orientations on purely hydrophilic MPMN surfaces. The multiplicity of binding orientations may explain the apparently large numbers of solvent-protected residues obtained by Bayraktar et al.’s NMR studies⁴⁴ for their hydrophilic MPMNs.

Binding Residues and the Role of Lysine. Several predominant contacting Cyt C residues have been highlighted in Figure 3 (hydrophobic residues italicized): OT Homo (Gln, *Ile*, *Phe*), 1:2 MH:OT (Lys, Asn, *Ile*, *Pro*), 1:1 MH:OT ‘thin’ (Lys, Gln, *Val*, *Phe*), 1:1 MH:OT ‘thick’ (Lys, *Val*, Tyr, Thr, Glu), 2:1 MH:OT (Lys, *Val*, *Phe*), and MH Homo (Lys, Glu). As noted above, hydrophilic residues appear to dominate binding to all MPMNs, with Gln contributing large percentages of contacts with OT Homo and 1:1 ‘thin’, Glu making substantial contributions to contacts with MH Homo. However, of particular note is lysine, which represents a large proportion of atomic contacts in all MPMN systems except the OT Homo (Figure 3 and Table 3). In the case of 2:1 MH:OT, lysine is responsible for 45% of all protein–MPMN contacts. The ability of lysine to form persistent contacts with all MPMN surfaces may stem from its side-chain structure, which consists of a hydrophobic alkyl portion (modeled here via a single hydrophobic bead) and a charged ‘head’ (modeled with a single charged bead); it is amphipathic, and thus capable of forming favorable interactions with both OT and MH. On mixed-composition surfaces, the hydrophobic and charged segments of the side chain can form simultaneous contacts with OT and MH, respectively. Indeed, lysine may favor binding near the boundary regions of well-defined, phase-separated hydrophobic/hydrophilic nanodomains, enabling simultaneous mixed interactions that are not possible on single ligand composition surfaces. In addition, the over-representation of lysine on the Cyt C surface may be responsible for the large increases in binding enthalpy with increasing %MH; as the amount of MH increases, more Cyt C lysine side chains are recruited to form additional favorable nonbonded interactions with the surface. For these reasons, lysine appears to play an important role in anchoring Cyt C to MPMN surfaces. A more detailed representation of the specific Cyt C residues contributing to atomic contacts in each of MPMN systems is summarized in Table 3 and depicted in bar charts presented in Figure S5 of Supporting Information.

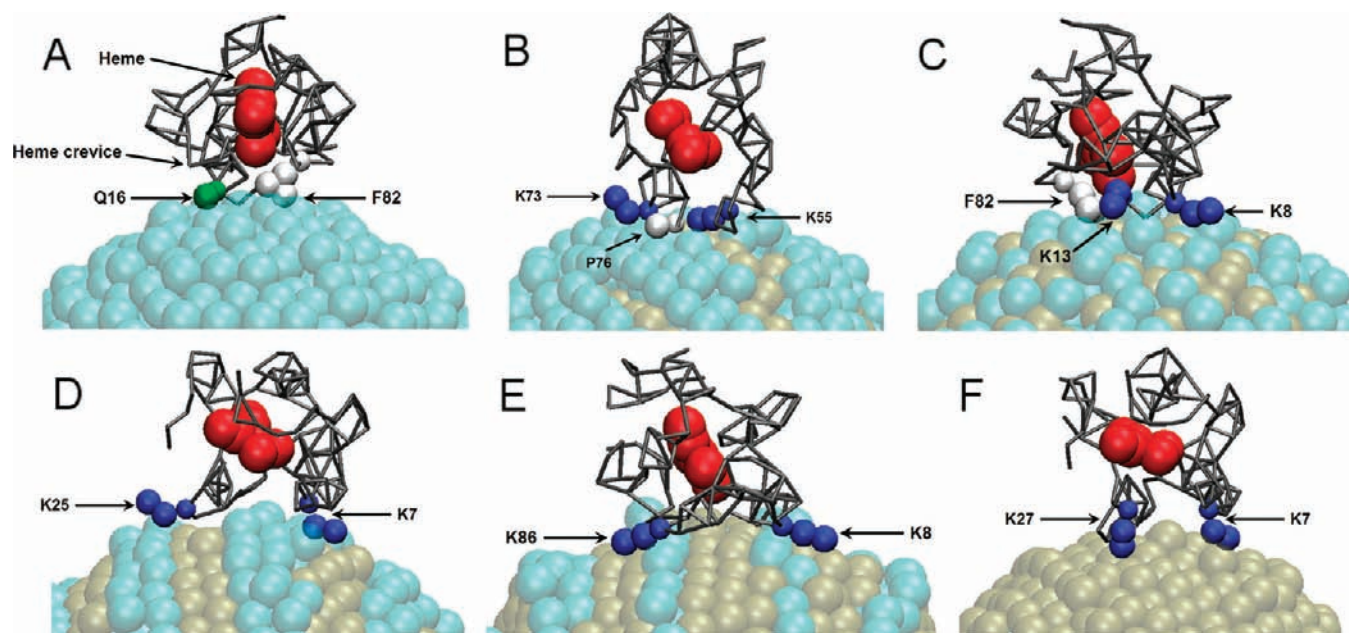


Figure 3. Lowest-energy binding conformations for the Cyt C–MPMN systems. (A) OT Homo, (B) 1:2 MH:OT, (C) 1:1 MH:OT ‘thin’, (D) 1:1 MH:OT ‘thick’ (E) 2:1 MH:OT, and (F) MH Homo MPMNs. Nanoparticle CG beads are colored according to the scheme outlined in Table 2. Cyt C particles are represented as follows: gray tubes represent protein backbone; CG model of HEME is shown using large, red spheres; residues which interact significantly with the NP are shown as spheres: generally, basic residues are shown in blue, acidic residues in red, uncharged polar residues in green, and hydrophobic residues (including aromatics) in white. Representative residues which make significant contacts with the surfaces, as determined by examination of contact profiles, are labeled and indicated by arrows.

Table 3. Atomic Contacts between Cyt C Residues and MPMN Surface Beads^a

amino acid (AA)	nanoparticles					
	OT Homo	1:2 MH:OT	1:1 MH:OT ‘thin’	1:1 MH:OT ‘thick’	2:1 MH:OT	MH Homo
Hydrophobic						
Ala	2.4%	3.4%	2.0%	5.8%	3.6%	3.1%
Cys	6.7%	-	3.1%	-	1.1%	-
Gly	-	5.2%	-	8.5%	1.7%	8.6%
Ile	15.1%	10.4%	4.1%	-	13.7%	-
Phe	21.8%	-	18.2%	2.2%	11.6%	0.5%
Pro	-	16.2%	-	-	-	-
Val	5.8%	---	10.3%	13.5%	2.4%	6.7%
Hydrophilic						
Asn	-	9.9%	-	-	-	-
Asp	-	2.3%	-	-	-	-
Glu	-	-	-	4.9%	5.0%	21.0%
Gln	34.8%	-	42.9%	11.2%	15.9%	1.6%
His	-	-	-	1.3%	-	0.1%
Lys	8.0%	26.1%	19.0%	33.0%	45.0%	41.0%
Thr	5.4%	2.2%	0.4%	10.9%	-	8.8%
Tyr	-	24.2%	-	8.7%	-	8.6%

^a Represents percentage of Cyt C–NP contacts made by specific amino acids over last 200 ns of MD simulations.

Figure S5 presents the atomic contact data in terms of hydrophobic and hydrophilic species present in both Cyt C and the MPMNs. Overall, the number of contacts made with hydrophilic residues increased with increasing MH content. Within the OT Homo system, a similar number of contacts were made by both hydrophobic and hydrophilic Cyt C residues (i.e., ~52% and 48%, respectively), while within the MH Homo system, a majority (~81%) of contacts were made by hydrophilic residues. However, for the mixed (‘striped’) MPMN systems, the number of contacts made by

hydrophilic residues remained relatively constant, averaging ~66% ± 3% over the MPMN MH content range of 33–67% (Figure S5B). Particularly interesting behavior was observed between the ‘thick’ and ‘thin’ 50% MH systems (1:1 MH:OT). These systems deviated by ~4% (i.e., thin, -4%; thick, +4%) from the average number of hydrophilic residue contacts observed within the striped MPMN systems.

OT and MH Contributions to Binding Enthalpies. To delineate the relative contributions of hydrophobic and hydrophilic

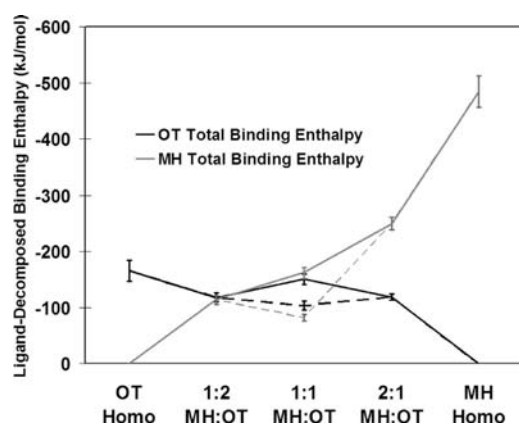


Figure 4. Contributions to the total protein–MPMN binding enthalpy from OT (black filled line) and MH (gray filled line) ligands. Dotted black and gray lines connect data point obtained for the 1:1 ‘thin’ MPMN OT and MH contributions, respectively.

interactions to the overall binding enthalpies for each CytC–MPMN system, we examined the interaction energies arising from contacts between the protein and OT and MH, separately. We note that hydrophilic interactions between the Cyt C and MH dominate protein–surface interactions, and the MH-dependent binding enthalpies exhibit simple monotonic behavior with respect to increasing MH fraction (Figure 4, gray filled line). For the 1:2 MH:OT MPMN, both ligands contribute approximately equally to protein binding, indicated by the crossover of the OT and MH binding enthalpy curves. However, MH contributes substantially more toward the binding enthalpy than OT for the “reverse-phase”, 2:1 MH:OT MPMN, which provides further indication of the dominance of hydrophilic interactions in Cyt C surface binding. In addition to MH content, we find that the relative contribution of OT and MH to overall binding varies depending on the stripe width. On the ‘thin’ 1:1 MH:OT surface, OT binds slightly more strongly to Cyt C compared to MH (with enthalpies of -103 and -82 kJ/mol, respectively), indicating that the relatively weak binding with MH allows the protein to interact more closely with OT. The opposite is observed for the ‘thick’ 1:1 MH:OT MPMN (OT = -151 , MH = -162 kJ/mol), suggesting that stronger binding with the MH stripes weakens the interaction with the OT stripes. The difference in binding enthalpies with OT and MH between the ‘thin’ and ‘thick’ MPMN surfaces may be explained in terms of interactions between the surface ligands and lysine, the main residue responsible for Cyt C adsorption as discussed above. The strong interaction between NH_3^+ and the MH domain on the ‘thick’ surface draws the hydrocarbon segment of the side chain away from the adjacent OT domain, resulting in strong MH but weak OT binding. For the ‘thin’ surface, the weaker binding of NH_3^+ to the MH domain (due to its narrowness and, thus, proximity to the neighboring hydrophobic OT stripe) enables the hydrocarbon segment (which is much longer) to be drawn toward the OT stripe, resulting in stronger OT binding.

Atomistic Simulations of Cyt C Adsorption: Comparisons with CG Simulations. We have performed atomistic simulations of Cyt C adsorption on pure OT, 1:1 ‘thin’, 1:1 ‘thick’ and pure MH model MPMN surfaces in order to clarify details of protein–surface interactions that are inaccessible to coarse-grained models. In particular, we sought to shed further light on the effects of stripe width on Cyt C binding. As discussed above, CG simulations predict that ‘thin’ striped MPMN surfaces exhibit weaker binding than ‘thick’ striped MPMN, despite their identical ligand composition.

Cyt C was found to adsorb to all four MPMN model surfaces, maintaining persistent contact with the surfaces throughout the duration of the simulated trajectories. We have calculated the binding enthalpies of the protein on each of the surfaces, decomposed separately into contributions from OT and MH ligands, shown in Table 4. We note that the values are of the same order of magnitude as those computed using the CG forcefield. With the exception of the 1:1 MH:OT ‘thin’ surface, there is a monotonic increase in binding enthalpy with respect to MPMN surface hydrophilicity (increasing %MH), in agreement with the CG simulations. This reinforces the importance of polar interactions (electrostatic and H-bonding interactions) in Cyt C adsorption. In addition to total binding enthalpy, we find that the relative contribution of OT and MH to overall binding varies depending on the stripe width. On the ‘thin’ striped surface, OT binds more strongly to Cyt C compared to MH (with enthalpies of -130 and -81 kJ/mol respectively). The opposite is true for the ‘thick’ surface (OT = -100 , MH = -322 kJ/mol), suggesting that the overwhelmingly stronger binding with the MH stripes weakens the interaction with the OT stripes. Conversely, for the ‘thin’ surface, the relatively weak binding with MH allows the protein to form more contacts with OT. The relative contributions of OT and MH to overall Cyt C binding enthalpies for the 1:1 MH:OT MPMN surfaces are consistent with those acquired from our CG simulations.

Our atomistic simulations reveal that the strength of Cyt C binding to mixed-ligand MPMN surfaces (as estimated by calculation of binding enthalpies) is directly related to (1) the total number of contacts between the protein and the surface; (2) the intimacy (closeness) and specificity (H-bonding) of these contacts; and (3) the extent of registry between the polar (and nonpolar) regions of the protein binding “face” and the corresponding MH and OT ligand nanostructure stripes. We discuss each of these factors in turn:

We identified the relative contributions of each of the Cyt C residues to surface interactions by inspection of the trajectory-averaged number of interatomic contacts between the protein and surface ligands for each of the modeled surfaces, displayed as bar charts in Figure 5. Inspection of Figure 5 indicates that, in general, Cyt C binding enthalpy is proportional to the total number of residue contacts with the surface (e.g., the homogeneous MH surface has by far the greatest total number of contacts). On the homogeneous OT surface (Figure 5A), interactions are dominated by Gln (Gln16), Lys (Lys25, 27, 79), and a cluster of C-terminal hydrophobic residues (Ile81, Phe82, Ala83). Similar residues are identified as capable of forming large numbers of contacts on the CG homogeneous OT nanoparticle surface (Figure 5SA). As in the CG simulations, of particular note is Lys which, although highly polar, nevertheless forms a high number of surface contacts. This can be explained by examination of the atomically detailed side chain of the atomistic simulation. Figure 6A shows a snapshot (at 50 ns) of Cyt C adsorbed onto the surface from the OT homo atomistic simulation, with Lys17 highlighted to illustrate side chain conformation. On the purely hydrophobic surface, the long hydrocarbon segment of the side chain is responsible for forming persistent contacts with the surface-exposed hydrocarbon (united) atom of the octane. On the 1:1 MH:OT ‘thin’ surface, Lys27 forms the largest number of contacts with the MH ligands (Figure 5B). As shown in Figure 6B, the lysine NH_3^+ group forms persistent bonds to the MH stripe, while at the same time, the methylene segment attaches to the adjacent OT stripe. Atomistic simulation

Table 4. Properties calculated from Atomistic Simulation Trajectories: Cyt C Binding Enthalpies (kJ/mol), Radii of Gyration (nm), Numbers of Protein-Surface Hydrogen Bonds, And Minimum Distance between Protein and Surface (nm)^a

	OT Homo	1:1 MH:OT 'thin'	1:1 MH:OT 'thick'	MH Homo
Binding Enthalpy (OT)	-297 (20)	-130 (12)	-100 (9)	N/A
(MH)	N/A	-81 (16)	-322 (50)	-781 (62)
(Total)	-297 (20)	-211 (22)	-422 (51)	-781 (62)
R_g	1.312 (0.007)	1.300 (0.007)	1.292 (0.006)	1.308 (0.009)
$R_g(x) \parallel$	0.99 (0.02)	0.99 (0.02)	1.127 (0.009)	1.05 (0.01)
$R_g(y) \parallel$	1.06 (0.01)	1.07 (0.01)	1.003 (0.008)	1.08 (0.02)
$R_g(z) \perp$	1.15 (0.01)	1.12 (0.01)	1.03 (0.01)	1.08 (0.01)
No. H-bonds	N/A	0.7 (0.7)	2.9 (1.4)	12.5 (2.7)
Minimum contact distance (OT)	0.28 (0.02)	0.30 (0.03)	0.34 (0.02)	N/A
(MH)	N/A	0.24 (0.06)	0.17 (0.01)	0.162 (0.006)

^a All quantities were averaged between 30-50 ns of the simulations. Values in parentheses indicate standard deviations.

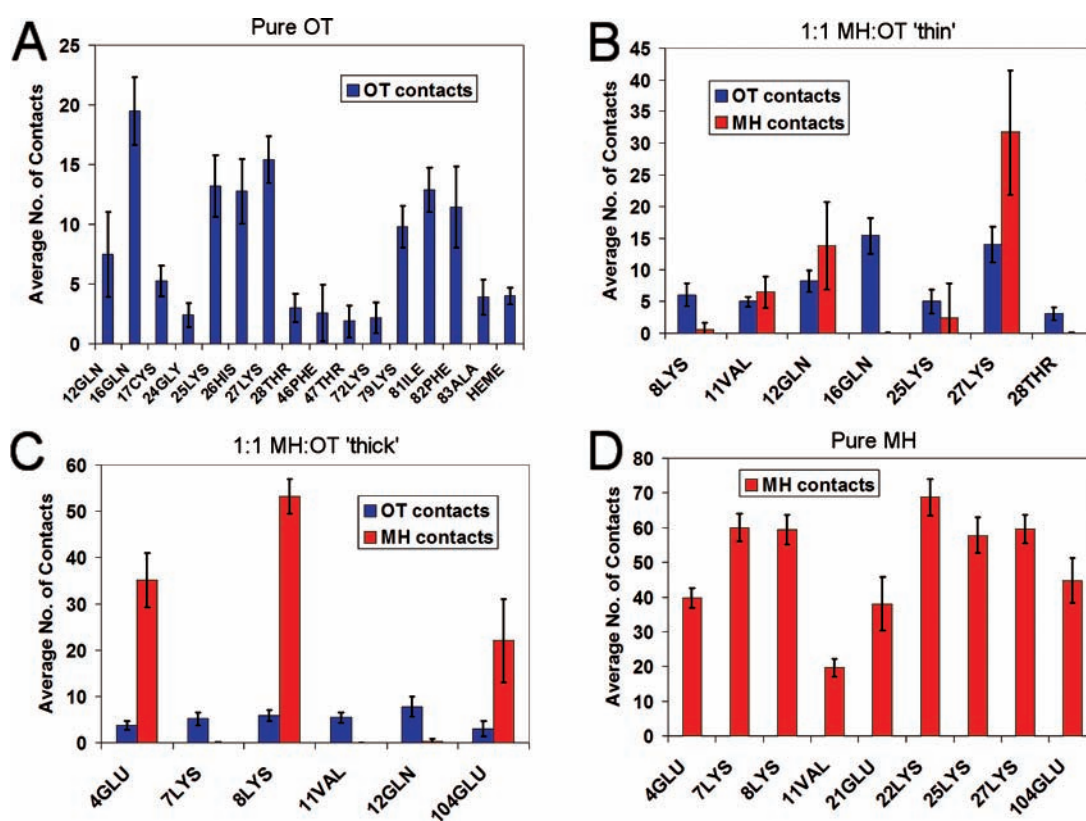


Figure 5. Bar graphs indicating numbers of contacts (within 0.45 nm) between surface ligands (OT or MH) and Cyt C residues calculated over 30–50 ns of the atomistic simulation trajectories, for (A) OT homogeneous; (B) 1:1 MH:OT 'thin'; (C) 1:1 MH:OT 'thick'; and (D) MH homogeneous model MPMN surfaces. Residues which form <1 contact are excluded.

of the MH Homo surface shows the same trend as that of the CG model, with Lys comprising the majority of surface contacts (5 residues in surface contact), while Glu represents the only other significant surface-binding hydrophilic residue (3 residues in surface contact).

The orientation of the Lys side chain is dependent on the composition and nanostructure of the ligand domains, adopting a parallel orientation along an extended hydrophobic surface with NH_3^+ pointing "up" (Figure 6A), while on mixed-ligand MPMN surfaces, specific, directional interactions with polar and non-polar ligand domains result in a preferred diagonal orientation at roughly 20° with respect to the surface plane, with the NH_3^+

group pointing "down" (Figure 6B,C). At the homogeneous MH MPMN surface, a large number of lysines form contacts (Figure 5D). Several of these are illustrated in the simulation snapshot of Figure 6D. The principal interaction is between the side chain NH_3^+ group and the surface-exposed $-\text{OH}$ group of the mercaptohexanol. However, due to the polarity of the MPMN surface, the hydrocarbon segment of the side chain is repelled, resulting in a more "upright" orientation compared to those observed on the other surfaces, with the side chain orientation angle of roughly 45° relative to the surface plane. We can now explain the difference in binding enthalpies between the 'thin' and 'thick' MPMN surfaces based on the knowledge that

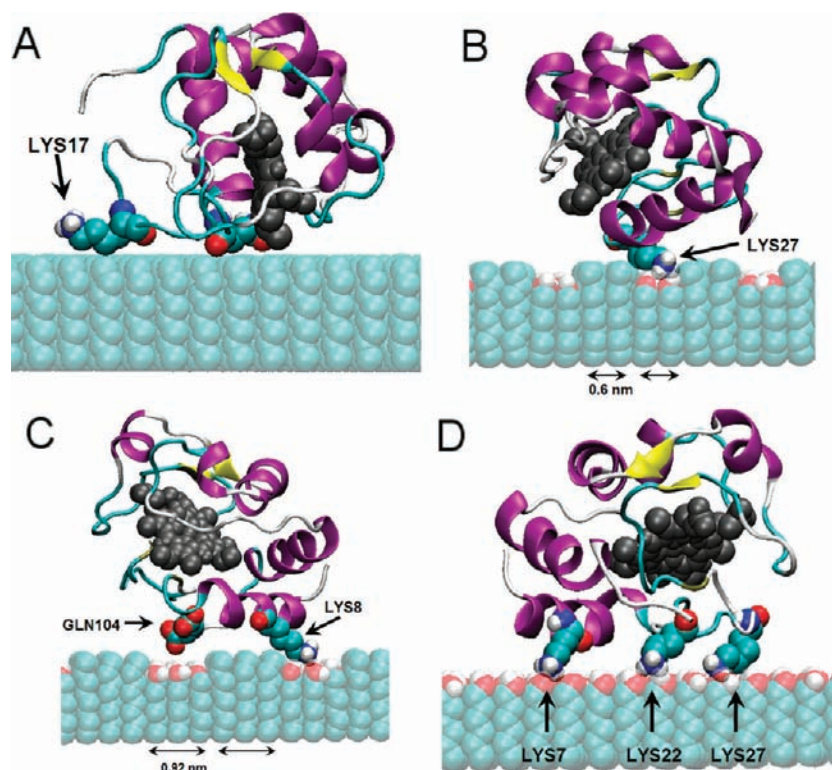


Figure 6. Atomistic simulation snapshots at 50 ns of Cyt C adsorbed onto (A) OT homogeneous; (B) 1:1 MH:OT ‘thin’; (C) 1:1 MH:OT ‘thick’; and (D) MH homogeneous model MPMN surfaces. Protein backbone shown in ribbon representation, heme group in metallic gray spheres, and representative residues which form significant contacts with the surfaces are shown as spheres and indicated.

lysine is the principal binding residue. The strong interaction between NH_3^+ and the MH domain on the ‘thick’ surface draws the hydrocarbon segment of the side chain away from the adjacent OT domain, resulting in strong MH but weak OT binding. For the ‘thin’ surface, the weaker binding of NH_3^+ to the MH domain (due to its narrowness, and thus, proximity to the neighboring hydrophobic OT stripe) enables the hydrocarbon segment (which is much longer) to be drawn toward the OT stripe, resulting in stronger OT binding.

We directly compared the contact profiles obtained from atomistic and CG simulations in order to determine the extent to which CG and AT simulations agree and to explore the validity of using a “flat” surface as a model of curved surfaces. We find that (as shown in Figure S6A and B), for the homogeneous OT and MH surfaces, the Cyt C residues that are in contact with the surfaces are similar for both curved and flat surfaces, indicating that the flat surface approximation is valid, at least for single-component ligand surfaces. This result also indicates that the CG model captures the salient features of Cyt C adsorption onto single-component ligand surfaces.

However, in the case of Cyt C adsorption on the 1:1 MH:OT MPMNs, differences between the CG and AT results merit further discussion (see Figure S6C,D). For the “thin” surface, both CG and AT simulations indicate involvement of residues 5–17 in surface binding (Figure S6C). The main difference is that, while the CG model predicts Phe82 making substantial contacts, the AT model predicts no surface contacts via Phe82, but instead, substantial surface contacts via Lys27. These two residues reside on opposite sides of residues 5–17 (illustrated in Figure S7A). Thus, r5–17 may be described as a stable “pivot” region, in close contact with the surface, about which the protein

may tilt. We note that in the initial orientation of Cyt C for the AT simulation, the placement was such that both Phe82 and Lys27 were in contact with the surface. During the course of the simulation, Cyt C reorients (tilts) such that Lys27 retains contact with the surface, while Phe82 is displaced to a more distant separation. Thus, in the AT model, there appears to be stronger repulsion between Phe and the polar surface ligands compared to the CG model. For the “thick” surface, both CG and AT models indicate involvement of residues 2–25 in surface binding (Figure S6D), although the AT model predicts much lower numbers of contacts for residues in the region r15–25. Visual inspection of the trajectory suggests that the region r15–25 is oriented toward the surface, but lies beyond the cutoff distance of 4.5 Å from the surface and thus is not defined as “in contact”. This proximity is illustrated in Figure S7B. The failure of r15–25 to make close contacts with the surface appears to be due to strong repulsion between Lys and the thick, nonpolar ligand domains. Given that the results obtained for the homogeneous MPMNs suggest that flat surfaces are a valid approximation for curved MPMNs, differences in the Cyt C binding mode for the 1:1 MH:OT MPMNs between the two simulation methods are likely to be mostly due to stronger polar/nonpolar group repulsion in the AT forcefield compared to the CG forcefield.

We also measured the “closeness” of the contacts between the protein and the MPMN surfaces by calculating trajectory-averaged values of the minimum distance between any atom of the protein and any atom of the surfaces, shown in Table 4. For Cyt C–OT ligand contacts, the tightest surface association occurs on the pure OT surface (with minimum distance of 0.28 ± 0.02 nm, characteristic of hydrophobic contacts), perhaps unsurprisingly, given the absence of polar surface ligands which may serve to

disrupt the hydrophobic interaction. Cyt C also forms a tighter association with OT on the 1:1 MH:OT 'thin' surface compared to that on the 'thick' surface (0.30 and 0.34 nm, respectively), consistent with the greater OT-dependent binding enthalpy of the former (discussed above). For the Cyt C–MH ligand contacts, there is a straightforward trend, with tighter protein–MH association with respect to increasing MH domain size/width. The association is strongest on the pure MH surface, with a minimum distance of 0.16 nm, characteristic of the presence of persistent H-bonding. Thus, the binding enthalpy is directly proportional to the overall tightness of association between the protein and the surface.

The binding enthalpy is also related to the capability of the MPMN surfaces to form hydrogen bonds with Cyt C, principally with lysine residues. Table 4 shows dramatic increases in the average number of protein–MH ligand H-bonds with respect to domain width. The 1:1 MH:OT 'thin' surface forms only one H-bond (with Lys27), which is weak, and the existence of which fluctuates wildly throughout the course of the trajectory, as indicated by the large standard deviation. In contrast, the 'thick' MPMN is capable of forming multiple H-bonds with Cyt C, with at least one H-bond present throughout the simulation. The pure MH surface forms many H-bonds with the protein. The tightness of residue-surface interactions is also evident in the standard deviations of the average number of contacts per residue over 20 ns segments of simulation as shown in Figure 5. For example, on the 1:1 'thin' surface, the Lys27-MH contact exhibits relatively high standard deviation (Figure 5B), suggestive of weaker binding, while the hydrophilic contacts on the 1:1 'thick' and the homogeneous MH surfaces (Figure 5C,D) exhibit much lower values of standard deviation, indicating stronger binding.

The stronger binding of Cyt C to the 1:1 MH:OT 'thick' surface may be related to the fortuitous alignment of the polar regions on the protein "face" which binds to the surface, and the locations of the corresponding hydrophilic ligand stripes on the MPMN. This is illustrated in Figure 7A, which shows that the areas on the protein binding interface populated by polar residues are approximately overlaid on the MH stripes, with the intervening nonpolar residues residing in between those stripes, that is, approximately on the OT ripple. The alignment is far from ideal, and there is undoubtedly polarity mismatch between the protein and the surface ligands. For lysine, though, mismatch is remedied by the capability of the side chain to optimize the interactions with both OT and MH (examples are shown in Figure 6B,C). A similar (approximate) alignment is shown for the 1:1 MH:OT 'thin' surface in Figure 7B. The polarity match is poorer than that of the 'thick' surface, with charged residues aligned with the two regions where the OT stripes reside (indicated by arrows at the top of the figure). However, in this case also, the inherent flexibility of the protein, coupled with side chain dynamics, enables the protein to adjust its structure to minimize the mismatch, albeit with a weaker match than that of the 'thick' MPMN surface. This result highlights the need for dynamical simulations in predictions of protein binding to nanopatterned surfaces. In this work, we have demonstrated that the flexibility of proteins and their side chains must be taken into account in order to reveal binding mechanisms and explain the interaction energetics.

Atomistic simulations also allow us to determine the extent to which adsorption onto different MPMN surfaces leads to structural deformation of the protein. Cyt C is relatively rigid, and there were no significant secondary structure changes in the

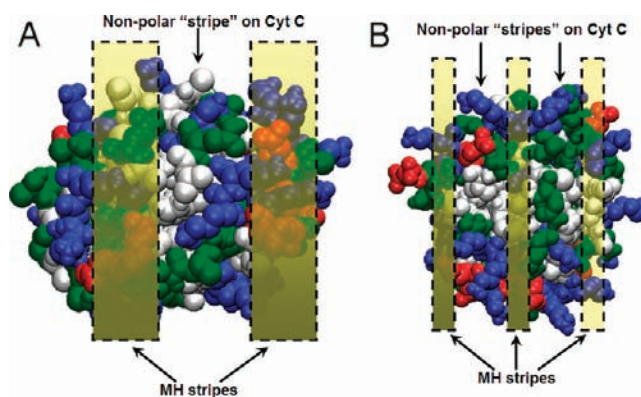


Figure 7. Snapshots of the surface-binding face of Cyt C on (A) 1:1 MH:OT 'thick'; and (B) 1:1 MH:OT 'thin' model MPMN surfaces. Protein atoms are given as spheres, color-coded according to residue type, with red = acidic, blue = basic, green = uncharged polar, and white = nonpolar. MH stripe locations are indicated by transparent yellow bars overlaid on the protein structures. Nonpolar "stripes" on the surface-binding face of Cyt C are indicated.

course of the 50 ns simulations for any of the systems (data not shown). Nevertheless, our simulations suggest that different MPMN surfaces affect the tertiary structure of the protein. We estimate the tertiary structure by examination of the radius of gyration (R_g), as well as the x , y and z components of R_g (Table 4), which provides insights into anisotropic structural deformations. Inspection of the R_g values indicate that adsorption onto the pure OT surface results in the greatest anisotropic deformation, with the difference between $R_g(z)$ (radius of gyration about a vector perpendicular to the surface plane) and $R_g(x)/(y)$ being greater than the other surfaces. This indicates that Cyt C adopts a "flat" shape upon adsorption, similar to that of a disc. A similar shape is adopted on the 1:1 MH:OT 'thin' surface, though to a lesser extent (i.e., the protein is less flat, but nevertheless roughly resembles a disc). This may be due to the relatively strong interaction between Cyt C and the hydrophobic OT ligands on this surface. For the homogeneous MH surface, all three components of R_g are approximately equal, indicating a roughly spherical shape, similar to that found in solution. This may be due to the fact that, although the MH surface makes the largest numbers of contacts with Cyt C, these contacts are largely via Lys, which extend out toward the surface, thus, keeping the bulk of the protein at length, whereas on the more hydrophobic surfaces, the bulk of the protein is more closely coupled to the surface, resulting in morphological changes (compression).

CONCLUSIONS

In this work, we have examined the interaction of Cyt C with nanostructured surfaces using experimental protein assays and computational molecular dynamics simulations. The nanostructured surfaces were formed from mixed MPMNs having hydrophilic/hydrophobic striped phase-separated domains less than 2 nm in width. Experimental microBCA assays revealed that overall adsorption of Cyt C generally increased with increasing %MH. Within the literature, increasing surface hydrophobicity is sometimes believed to be the single direct explanation for increasing protein adsorption at surfaces.^{45,46} However, for Cyt C, increasing surface *hydrophilicity* enhances protein adsorption, highlighting the need to take into full account the physicochemical and structural characteristics of the protein under consideration

when attempting to produce predictive models of biomolecule adsorption on complex surfaces.

Protein–surface adsorption enthalpies calculated from computational simulations employing a semirigid coarse-grained protein/nanoparticle model indicate an overall increase in adsorption strength with respect to %MH, in qualitative agreement with the microBCA results. This finding suggests that Cyt C does not undergo significant structural disruption while interacting with an MPMN surface. Furthermore, our results suggest that a simplified, CG semirigid body model is applicable to studying surface adsorption of small, globular proteins with structural stability comparable to that of Cyt C.

One of the key conclusions to emerge from our modeling studies is the important role of Lys in facilitating Cyt C adsorption to MPMN surfaces. The amphipathic character of the Lys side chain enables it to form close contacts with both polar and nonpolar surface ligands simultaneously, rendering it especially important for interactions with surfaces composed of nanoscale chemical domains. We also note that another basic amino acid, Arg, may exhibit a similar capacity for “dual binding” (although possibly to a lesser extent, due to weaker hydrophobic interactions), provided that the surface nanostructure exhibits polar/nonpolar domains with sizes commensurate to those of the side chain. However, Arg is not present on the wild-type Cyt C surface, and therefore, no direct observation can be drawn from the present study. We suggest that unnatural amino acids can be designed with specific size and dual affinity in mind to facilitate design of engineered proteins exhibiting enhanced adsorption onto nanostructured surfaces.

With an understanding of how the nature of surfaces (i.e., nanostructuring) influences protein dynamics, control of their bound states can be achieved. This may give rise to an array of newly tailored materials/surface coatings for use as biosensors, hybrid materials, nanotechnology, and biocompatible surfaces. Of particular current interest is the control over bioactivity or cell adhesion that can result from fine-tuning of surface coatings.

■ ASSOCIATED CONTENT

S Supporting Information. Additional experimental details of NP synthesis and further details of simulation parameters. NP characterization results from contact angle, AFM and TEM measurements. More detailed results from coarse-grained and atomistic simulations. This material is available free of charge via the Internet at <http://pubs.acs.org>.

■ AUTHOR INFORMATION

Corresponding Author

m.stevens@imperial.ac.uk; irene.yarovsky@rmit.edu.au

■ ACKNOWLEDGMENT

M.M.S. thanks the Engineering and Physical Science Research Council (EPSRC), U.K., and European Research Council (ERC) grant *Naturelle* for funding. A.H. and I.Y. thank the Victorian Partnership for Advanced Computing (VPAC), the National Computational Infrastructure (NCI), and the Victorian Life Sciences Computation Initiative (VLSCI) for provision of computational facilities. S.M. would like to acknowledge the Natural Sciences and Engineering Research Council of Canada (NSERC) for providing him with the funding support to conduct this research.

■ REFERENCES

- (1) Andersson, M.; Madgavkar, A.; Stjern Dahl, M.; Wu, Y. R.; Tan, W. H.; Duran, R.; Niehren, S.; Mustafa, K.; Arvidson, K.; Wennerberg, A. *Rev. Sci. Instrum.* **2007**, *78*.
- (2) Vogler, E. A. *Adv. Colloid Interface Sci.* **1998**, *74*, 69–117.
- (3) Vogler, E. A. *J. Biomater. Sci., Polym. Ed.* **1999**, *10*, 1015–1045.
- (4) Mrksich, M.; Whitesides, G. M. *Annu. Rev. Biophys. Biomol. Struct.* **1996**, *25*, 55–78.
- (5) Templeton, A. C.; Wuelfing, M. P.; Murray, R. W. *Acc. Chem. Res.* **2000**, *33*, 27–36.
- (6) Centrone, A.; Hu, Y.; Jackson, A. M.; Zerbi, G.; Stellacci, F. *Small* **2007**, *3*, 814–817.
- (7) Centrone, A.; Penzo, E.; Sharma, M.; Myerson, J. W.; Jackson, A. M.; Marzari, N.; Stellacci, F. *Proc. Natl. Acad. Sci. U.S.A.* **2008**, *105*, 9886–9891.
- (8) Jackson, A. M.; Myerson, J. W.; Stellacci, F. *Nat. Mater.* **2004**, *3*, 330–336.
- (9) Jackson, A. M.; Hu, Y.; Silva, P. J.; Stellacci, F. *J. Am. Chem. Soc.* **2006**, *128*, 11135–11149.
- (10) Uzun, O.; Hu, Y.; Verma, A.; Chen, S.; Centrone, A.; Stellacci, F. *Chem. Commun.* **2008**, 196–198.
- (11) Verma, A.; Uzun, O.; Hu, Y. H.; Hu, Y.; Han, H. S.; Watson, N.; Chen, S. L.; Irvine, D. J.; Stellacci, F. *Nat. Mater.* **2008**, *7*, 588–595.
- (12) Singh, C.; Ghorai, P. K.; Horsch, M. A.; Jackson, A. M.; Larson, R. G.; Stellacci, F.; Glotzer, S. C. *Phys. Rev. Lett.* **2007**, *99*.
- (13) DeVries, G. A.; Brunnbauer, M.; Hu, Y.; Jackson, A. M.; Long, B.; Neltner, B. T.; Uzun, O.; Wunsch, B. H.; Stellacci, F. *Science* **2007**, *315*, 358–361.
- (14) Cassie, A.; Baxter, S. *Trans. Faraday Soc.* **1944**, *40*, 546–551.
- (15) Kuna, J. J.; Voitchovsky, K.; Singh, C.; Jiang, H.; Mwenifumbo, S.; Ghorai, P. K.; Stevens, M. M.; Glotzer, S. C.; Stellacci, F. *Nat. Mater.* **2009**, *8*, 837–842.
- (16) Eggleston, C. M.; Khare, N.; Lovelace, D. M. *J. Electron Spectrosc.* **2006**, *150*, 220–227.
- (17) Castellini, E.; Ranieri, A.; Simari, D. A.; Di Rocco, G. *Langmuir* **2009**, *25*, 6849–6855.
- (18) Zheng, N.; Fan, J.; Stucky, G. D. *J. Am. Chem. Soc.* **2006**, *128*, 6550–6551.
- (19) Mahapatro, A. K.; Scott, A.; Manning, A.; Janes, D. B. *Appl. Phys. Lett.* **2006**, *88*.
- (20) Brust, M.; Bethell, D.; Kiely, C. J.; Schiffrin, D. J. *Langmuir* **1998**, *14*, 5425–5429.
- (21) Musick, M. D.; Keating, C. D.; Keefe, M. H.; Natan, M. J. *Chem. Mater.* **1997**, *9*, 1499–8.
- (22) Shipway, A. N.; Katz, E.; Willner, I. *ChemPhysChem* **2000**, *1*, 18–52.
- (23) Young, T. *Philos. Trans. R. Soc. London* **1804**, *94*, 1–16.
- (24) Thermo Scientific, Rockford, IL, 1986.
- (25) Yang, L.; Li, L.; Tu, Q.; Ren, L.; Zhang, Y.; Wang, X.; Zhang, Z.; Liu, W.; Xin, L.; Wang, J. *Anal. Chem.* **2010**, *82*, 6430–6439.
- (26) Lindahl, E.; Hess, B.; van der Spoel, D. *J. Mol. Model.* **2001**, *7*, 306–317.
- (27) Van der Spoel, D.; Lindahl, E.; Hess, B.; Groenhof, G.; Mark, A. E.; Berendsen, H. J. C. *J. Comput. Chem.* **2005**, *26*, 1701–1718.
- (28) Marrink, S. J.; Risselada, H. J.; Yefimov, S.; Tieleman, D. P.; de Vries, A. H. *J. Phys. Chem. B* **2007**, *111*, 7812–7824.
- (29) Monticelli, L.; Kandasamy, S. K.; Periole, X.; Larson, R. G.; Tieleman, D. P.; Marrink, S. J. *J. Chem. Theory Comput.* **2008**, *4*, 819–834.
- (30) Marrink, S. J.; de Vries, A. H.; Mark, A. E. *J. Phys. Chem. B* **2004**, *108*, 750–760.
- (31) Bushnell, G. W.; Louie, G. V.; Brayer, G. D. *J. Mol. Biol.* **1990**, *214*, 585–595.
- (32) Berman, H. M.; Westbrook, J.; Feng, Z.; Gilliland, G.; Bhat, T. N.; Weissig, H.; Shindyalov, I. N.; Bourne, P. E. *Nucleic Acids Res.* **2000**, *28*, 235–242.
- (33) Oostenbrink, C.; Villa, A.; Mark, A. E.; Van Gunsteren, W. F. *J. Comput. Chem.* **2004**, *25*, 1656–1676.

- (34) Oostenbrink, C.; Soares, T. A.; van der Vegt, N. F. A.; van Gunsteren, W. F. *Eur. Biophys. J.* **2005**, *34*, 273–284.
- (35) Berendsen, H. J. C.; Postma, J. P. M.; van Gunsteren, W. F.; Hermans, J. In *Intermolecular Forces*; Pullman, B., Ed. Reidel: Dordrecht, 1981; p 331.
- (36) Futamura, K.; Matsuno, R.; Konno, T.; Takai, M.; Ishihara, K. *Langmuir* **2008**, *24*, 10340–10344.
- (37) Li, D.-F.; Wang, H.-J.; Fu, J.-X.; Wang, W.; Jia, X.-S.; Wang, J.-Y. *J. Phys. Chem. B* **2008**, *112*, 16290–16299.
- (38) Mun, K.-S.; Alvarez, S. D.; Choi, W.-Y.; Sailor, M. J. *ACS Nano* **2010**, *4*, 2070–2076.
- (39) Gorbenko, G. P.; Domanov, Y. A. *Biophys. Chem.* **2003**, *103*, 239–249.
- (40) Domanov, Y. A.; Molotkovsky, J. G.; Gorbenko, G. P. *Biochim. Biophys. Acta, Biomembr.* **2005**, *1716*, 49–58.
- (41) Gorbenko, G. P.; Molotkovsky, J. G.; Kinnunen, P. K. J. *Biophys. J.* **2006**, *90*, 4093–4103.
- (42) Trzaskowski, B.; Leonarski, F.; Les, A.; Adamowicz, L. *Bio-macromolecules* **2008**, *9*, 3239–3245.
- (43) Talasaz, A. H.; Nemat-Gorgani, M.; Liu, Y.; Stahl, P.; Dutton, R. W.; Ronaghi, M.; Davis, R. W. *Proc. Natl. Acad. Sci. U.S.A.* **2006**, *103*, 14773–14778.
- (44) Bayraktar, H.; You, C. C.; Rotello, V. M.; Knapp, M. J. *J. Am. Chem. Soc.* **2007**, *129*, 2732–+.
- (45) Absolom, D. R.; Zingg, W.; Neumann, A. W. *J. Biomed. Mater. Res.* **1987**, *21*, 161–171.
- (46) Jonsson, U.; Ivarsson, B.; Lundstrom, I.; Berghem, L. *J. Colloid Interface Sci.* **1982**, *90*, 148–163.